

Article

Pure Aluminum Structure and Mechanical Properties Modified by Al₂O₃ Nanoparticles and Ultrasonic Treatment

Ilya A. Zhukov ¹, Alexander A. Kozulin ¹, Anton P. Khrustalyov ^{1,2,*} , Nikolay I. Kahidze ¹, Marina G. Khmeleva ¹ , Evgeny N. Moskvichev ^{1,2}, Dmitry V. Lychagin ¹ and Alexander B. Vorozhtsov ¹

¹ National Research Tomsk State University, Lenin av. 36, 634050 Tomsk, Russia; gofra930@gmail.com (I.A.Z.); kzln2015@yandex.ru (A.A.K.); nick200069@yandex.ru (N.I.K.); khmelmg@gmail.com (M.G.K.); em_tsu@mail.ru (E.N.M.); lychagindv@mail.ru (D.V.L.); abv1953@mail.ru (A.B.V.)

² Institute of Strength Physics and Materials Science of the Siberian Branch of the Russian Academy of Sciences, pr. Akademicheskii 2/4, 634055 Tomsk, Russia

* Correspondence: tofik0014@mail.ru; Tel.: +7-952-155-55-68

Received: 13 October 2019; Accepted: 6 November 2019; Published: 7 November 2019



Abstract: This paper examines dispersion hardened alloys based on commercial-purity aluminum obtained by permanent mold casting with the addition of aluminum oxide nanoparticles. Ultrasonic treatment provides a synthesis of non-porous materials and a homogeneous distribution of strengthening particles in the bulk material, thereby increasing the mechanical properties of pure aluminum. It is shown that the increase in the alloy hardness, yield stress, ultimate tensile strength, and lower plasticity depend on the average grain size and a greater amount of nanoparticles in the alloy.

Keywords: aluminum; alumina nanoparticles; microstructure; mechanical properties; elastic limit; strength

1. Introduction

The development of aerospace and automotive industries is accompanied by increased requirements for the materials applied, in particular, high specific strength, workability, and low cost [1,2]. Conventional aluminum alloys do not fully meet these requirements. For example, zirconium- and scandium-containing alloys currently used in industry possess the appropriate level of mechanical properties but are rather expensive [3–5]. Consequently, new, lightweight metal-based materials with the required properties are being intensively developed.

The use of metal matrix composites seems to be relevant [1,6,7] because the mechanical properties of such composites can be improved by the addition of high-melting particles, including ceramic nanoparticles [8–13]. There are different methods of manufacturing such materials, but casting technologies are the most universal and efficient [14,15]. At the same time, the production of composite materials using casting technology is connected with a spectrum of problems concerning particle agglomeration and flotation due to low wettability with melt [16–19]. As a result, the composite density lowers, and the structure becomes non-homogeneous, leading to a decrease in the mechanical properties of the material. This problem can be solved by several methods, namely the coating deposition onto particles to enhance wettability [20], the addition of a master alloy, and the exposure of molten metal to external effects. One such effect is the ultrasonic melt treatment. As is known, the ultrasonic treatment provides melt degassing and also allows the introduction and distribution of nanoparticles owing to their wettability and deagglomeration. These uniformly distributed nanoparticles promote structural

refinement and harden the material. Structural refinement occurs due to the melt overcooling around the introduced particles on which grains start to grow. Dispersion hardening is achieved by the particle's ability to resist dislocation motion during deformation. This requires additional energy to overcome these barriers.

In most publications focused on the investigation of the nanoparticle effect on the structure and properties of aluminum, a small amount (not over 0.5 wt.%) of additives was used alongside base alloys with complex chemical compositions. For example, Vorozhtsov et al. [21] introduced non-metallic nanoparticles via an A356 aluminum alloy. This allowed them to significantly increase the yield stress, ultimate tensile strength, and plasticity of the alloy. The difference in the thermal-expansion coefficients of the matrix and nanoparticles made the most important contribution to the improvement of the mechanical properties of the alloy. At the same time, the presence of other elements in alloys prevents one from fully appreciating the contribution of nanoparticles in matrix deformation and failure.

The aim of this work is to explore the influence of different amounts of aluminum oxide (Al_2O_3) nanoparticles on the structure and mechanical properties of pure aluminum.

2. Materials

2.1. Preparation of Nanoparticles

Al_2O_3 nanoparticles were used in this experiment as a hardener. They were obtained by the electrical explosion of wire [22]. The structure, particle distribution histogram, and phase composition of the initial Al_2O_3 nanoparticles are shown in Figure 1.

Al_2O_3 nanoparticles and aluminum powder (20 μm) were mixed with the addition of 200 mL petroleum ether and 1.5 wt.% octadecanoic acid as a superficially active substance to provide deagglomeration and homogeneous distribution of the nanoparticles. After 20 min of mixing, the powder composition was air-dried and then sifted. The powder composition was wrapped in foil to achieve a cylindrical package. The prepared powder mixture was then introduced to the melt.

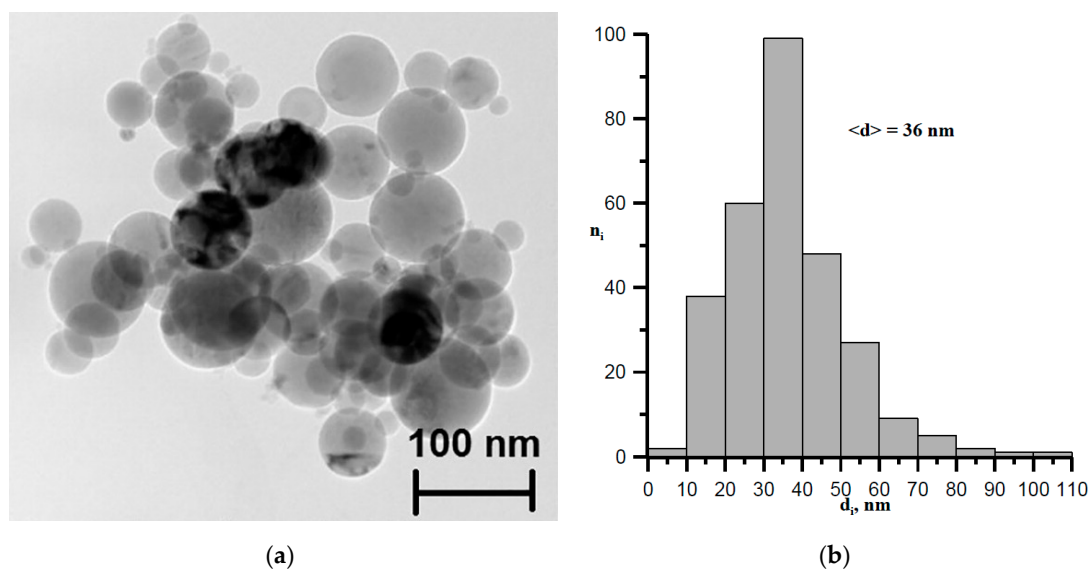


Figure 1. Cont.

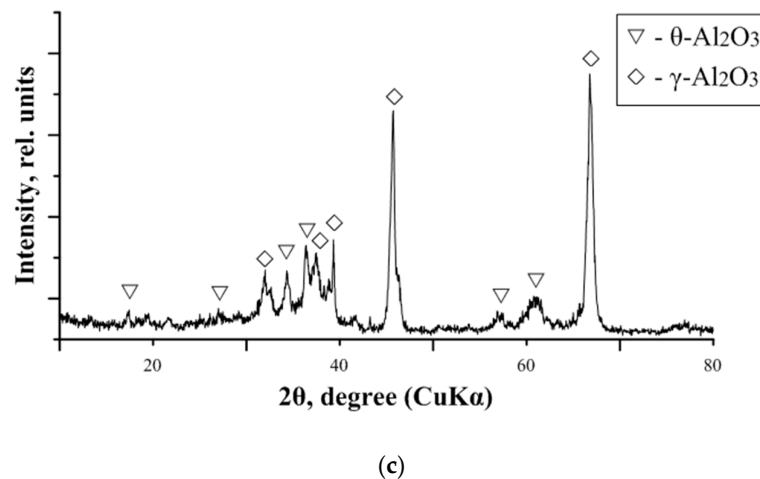


Figure 1. TEM image of the structure (a), particle distribution histogram (b), and powder X-ray diffraction [22] (c) of the Al_2O_3 nanoparticles.

2.2. Alloy Casting

The 1100 aluminum alloy (99.0 wt.% Al, 0.8 wt.% Si, 0.04 wt.% Mg) castings were prepared in a laboratory-scale melter with the addition of master alloy containing ceramic Al_2O_3 nanoparticles. The ultrasonic treatment (UST) for 2 min, and the addition of the master alloy was carried out simultaneously at 730 °C. The aluminum alloy melt was prepared at 1003 K in an electric furnace, in a clay graphite crucible. The permanent mold casting in a $100 \times 150 \times 10 \text{ mm}^3$ steel die was then used to obtain the cast products. Prior to experimental research, the cast products were annealed at 300 °C for one hour. Alloys with nanoparticles of aluminum oxide were also obtained without using ultrasonic treatment (no UST).

3. Methods

The electron backscatter diffraction (EBSD) technique for a Tescan Vega II LMU scanning electron microscope (SEM) (TESCAN ORSAY HOLDING, Brno, Czech Republic) was used to study the grain structure and orientation of the alloy surface. The surface was prepared by mechanical polishing and ion milling on a SEMPRep2 multifunction device (Technoorg Linda Co. Ltd., Budapest, Hungary). The EBSD analysis of the obtained data was performed via HKL Channel 5 software (Oxford Instruments, High Wycombe, UK).

In accordance with the ASTM E-8M-08 standard, the plate-like samples had 25 mm gauge length, 2 mm thickness, 6 mm width, and 14 mm spherical radius and were obtained via electrical discharge machining. The samples were used for uniaxial tension testing on an Instron 3369 Dual Column Tabletop Testing System (Instron European Headquarters, HighWycombe, UK) conducted at 24 °C with a 0.001 s^{-1} strain rate.

The Brinell hardness test method was used to determine the Brinell hardness, as defined in the ASTM E103 standard, using a wide sample surface in different places. For hardness measurements, a Duramin 500 (Struers GmbH, Ballerup, Denmark) hardness tester was used. Measurements were carried out at a 2500 N indentation load over 30 s. More than 20 measurements were performed for each sample. The sample surface was prepared in accordance with the standard procedures for abrasive machining.

4. Experimental Results

The grain structure and the grain size distribution in the studied alloys are illustrated in Figure 2. The average grain size of the initial Al 1100 alloy is 200 μm . The grain size of 112 and 69 μm belongs to the dispersion-hardened alloys with 0.5 and 1 wt.% Al_2O_3 , respectively.

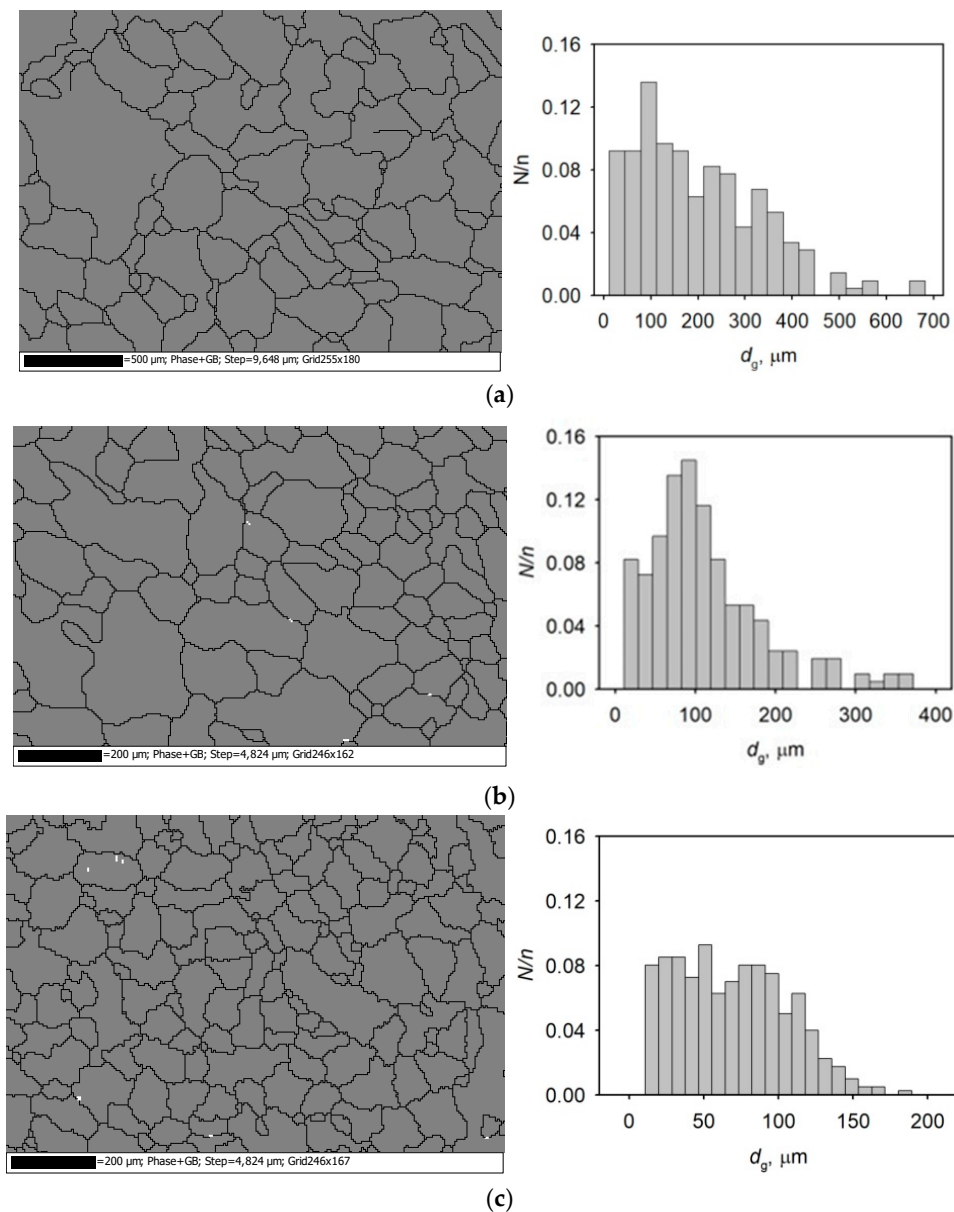


Figure 2. EBSD images of the structure and block diagrams of the grain size distribution in the alloy samples: (a) initial state, (b) 0.5 wt.% Al_2O_3 , (c) 1 wt.% Al_2O_3 . d_g is the grain size, and N/n is the ratio between the number of measurements and the number of grains of a certain size.

The results of the Brinell hardness tests are shown in Figure 3.

As can be seen from Figure 3, the Brinell hardness increases with an increasing content of hardening nanoparticles and decreasing average grain size. Its maximum value of 21.7 HBW is observed after the addition of 1 wt.% Al_2O_3 . The increased content of 1.5 wt.% Al_2O_3 does not change the alloy hardness. The addition of 0.1 wt.% Al_2O_3 without ultrasonic treatment produces an insignificant hardness increase from 18.5 to 19.6 HBW. A further increase in Al_2O_3 content lowers the alloy hardness because the nanoparticle distribution in aluminum cannot be reached without ultrasonic treatment.

The stress–strain curves resulting from the uniaxial tensile tests are presented in Figure 4.

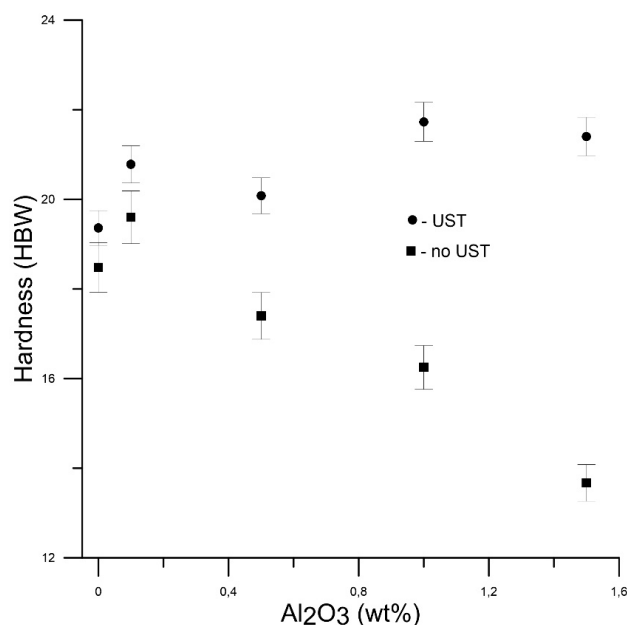


Figure 3. The dependence between the Brinell hardness and Al₂O₃ content in the 1100 aluminum alloy.

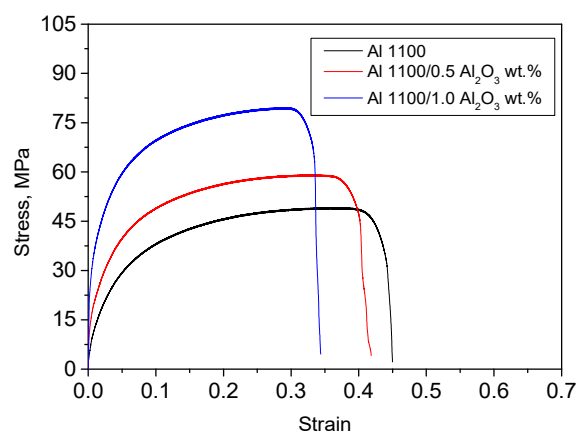


Figure 4. Stress–strain curves obtained for the tensile test samples from investigated alloys: Al 1100: Initial state; Al 1100/0.5 wt.% Al₂O₃; Al 1100/1 wt.% Al₂O₃.

Table 1 presents the mechanical properties of aluminum alloys with different amounts of Al₂O₃ nanoparticles. According to this table, when the content of Al₂O₃ nanoparticles increased to 1 wt.%, the yield stress (YS) and the ultimate tensile strength (UTS) grew from 12 to 27 MPa and from 48.75 to 79.1 MPa, respectively. The growth of YS and UTS led the plasticity to reduce from 45% to 34.4%.

Table 1. Mechanical properties of the investigated alloys.

Alloy Composition	$P \times 10^3, \text{g/mm}^3$	YS, MPa	UTS, MPa	$\epsilon_{\text{max}}, \%$	Brinell Hardness
Initial state	2.68	12.08	48.75	45	19.36
0.5 wt.% Al ₂ O ₃	2.66	16.36	58.85	41.8	20.08
1 wt.% Al ₂ O ₃	2.69	27.40	79.10	34.4	21.73

Figure 5 shows the yield stress (YS) and the ultimate tensile stress (UTS), which are dependent on the concentration of Al₂O₃ nanoparticles in the 1100 aluminum alloy.

As shown in Figure 5, the addition of Al₂O₃ nanoparticles with ultrasonic treatment in the amount of 0.1 wt.% significantly increased both the yield stress and the ultimate tensile stress. Al₂O₃ nanoparticles introduced in an amount over 0.1 wt.% decreases the yield stress. The ultimate tensile

stress is the same. The addition of Al₂O₃ nanoparticles without ultrasonic treatment does not allow enhancement of the mechanical properties of the alloy. One can see the reduction in the yield stress from 8 to 4 MPa, the ultimate tensile stress from 35 to 16 MPa, and the plasticity from 35% to 5%.

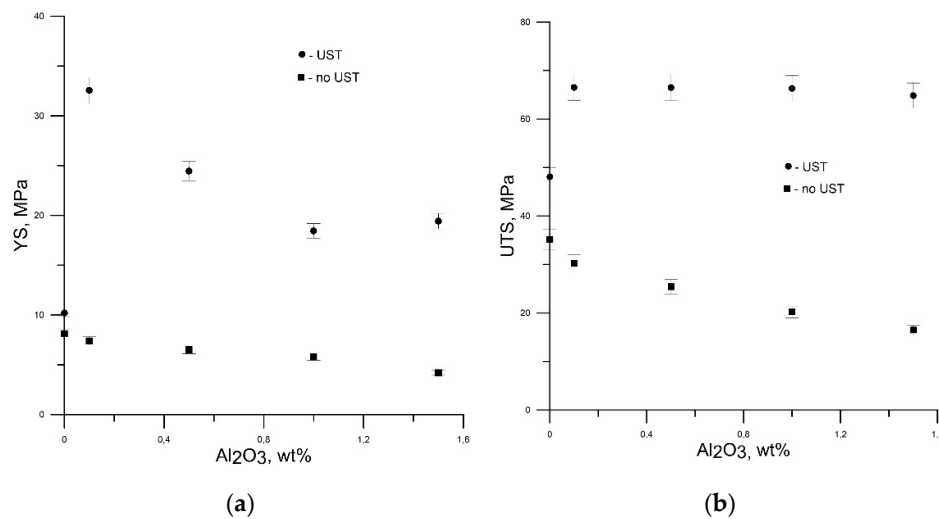


Figure 5. The dependencies of (a) the yield stress (YS) and (b) the ultimate tensile stress (UTS) depending on the Al₂O₃ nanoparticle concentration in the 1100 aluminum alloy.

5. Discussion

The investigation results of the alloy microstructure show that the presence of Al₂O₃ nanoparticles in the melt affects the grain size. This is because the melt–nanoparticle system is in a low-stability state. Therefore, any thermal effects on the grain nucleation from inoculant particles modify the aggregate state of the melt on their surface. As a result, the matrix starts to crystallize, and decreases the size of the grain nucleus, thus forming a lower grain size. A homogeneous distribution of inoculant particles in the melt provides the formation of a uniform structure in the bulk material.

The significant improvement of the mechanical properties of pure aluminum can be explained by the influence of four hardening mechanisms: The Hall–Petch relationship, Orowan strengthening, the particle-to-matrix load transfer, and the material hardening owing to the difference between the thermal-expansion coefficients of the particles and the aluminum matrix.

5.1. Hall–Petch Relationship

The contribution of grain refinement to the improvement of the mechanical properties of the material can be calculated by the Hall–Petch relationship [23]:

$$\sigma_{GR} = k_y(D^{-\frac{1}{2}} - D_0^{\frac{1}{2}}), \quad (1)$$

where D and D_0 are the grain size, and k_y is the Hall–Petch coefficient (~68 MPa).

In accordance with the Hall–Petch relationship, the addition of 0.5 and 1 wt.% Al₂O₃ enhances the mechanical properties of pure aluminum by 2.4 and 3.7 MPa, respectively.

5.2. Orowan Strengthening

The Orowan strengthening mechanism implies the direct influence of homogeneously distributed solid particles on precipitation hardening. These particles impede the smooth motion of dislocations through the matrix over its slip planes. When the particle size is greater than 1 μm, this effect can be neglected [1]. The increase in precipitation hardening is in inverse proportion to the distance between particles. Thus, the smaller the particles, the stronger the hardening. The latter can be achieved

in an inverse proportion to the volume fraction of particles. The contribution of Orowan [24,25] strengthening to the mechanical properties of the alloy can be obtained from

$$\sigma_{OR} = \frac{0.13bG_m}{\lambda} \ln \frac{d_p}{2b} \quad (2)$$

where λ is the geometry of the distance between particles. This value is calculated as

$$\lambda = d_p \left(\left(\frac{1}{2V_p} \right)^{\frac{1}{3}} - 1 \right) \quad (3)$$

where b is the Burgers vector, G_m is the shear modulus, d_p is the mean diameter of nanoparticles, and V_p is the volume fraction of the particles.

In accordance with Orowan strengthening, the addition of 0.5 and 1 wt.% Al₂O₃ allows us to improve the mechanical properties of pure aluminum, respectively, by 19.7 and 36.4 MPa.

5.3. Particle-to-Matrix Load Transfer

The particle-to-matrix load transfer is caused by the direct particle contribution to the hardening process. This particle contribution depends on the amount in the alloy and can be written as [16]

$$\sigma_{load} = 0.5V_p\sigma_m, \quad (4)$$

where V_p is the volume fraction of Al₂O₃ nanoparticles, and σ_m is the yield stress of the matrix alloy (12 MPa).

The calculated load transfer is 2.16 and 4.32 MPa for 0.5 and 1 wt.% Al₂O₃, respectively.

5.4. Difference between the Thermal-Expansion Coefficients of the Particles and Aluminum Matrix

When the alloy temperature drops to room temperature, volume inconsistency between the matrix and strengthening particles can be produced by the difference between their thermal-expansion coefficients. This subsequently leads to the formation of dislocations around the strengthening particles. The length of the generated dislocation loop is determined by the value of πd_p (d_p is the particle size). Material hardening due to the difference in thermal-expansion coefficients can then be evaluated as [16]

$$\Delta\sigma_{CTE} = \beta G b \left(\frac{12(\alpha_m - \alpha_p)\Delta T V_p}{b d_p (1 - V_p)} \right)^{\frac{1}{2}} \quad (5)$$

where β is the constant (~1.25), α_m is the thermal-expansion coefficient of the Al matrix (23×10^{-6} 1/K), α_p is the thermal-expansion coefficient of the strengthening particles (7×10^{-6} 1/K), and ΔT is the difference between the synthesis (725 °C) and room (25 °C) temperatures. The value of d_p is used here as an average distance between the particles (~1.8 μ m) calculated for the alloy sample with 1 wt.% Al₂O₃. This is shown in Figure 6.

$$G = 0.5E_m / (1 + \nu) \quad (6)$$

where E_m is the Young's modulus for aluminum (70 GPa), ν is the Poisson ratio (0.33), and b is the Burgers vector (0.286 nm). The difference in the thermal-expansion coefficients calculated for the alloy sample with 1 wt.% Al₂O₃ is 20 MPa. Based on the results obtained, it can be concluded that in introducing Al₂O₃ nanoparticles to pure aluminum, the Orowan strengthening and the difference in a uniform thermal-expansion coefficients of the matrix and the particles dominate among other indicated mechanisms of precipitation hardening.

For pure aluminum, the picture is observed when the introduction of nonmetallic inclusions increases the yield strength, tensile strength, and decreases the plasticity, which corresponds to the

results presented in [2,14,26,27]. Moreover, the introduction of nanoparticles, including aluminum oxide, into aluminum alloys can lead to a simultaneous increase in plasticity [21,28–30]. All this indicates that the alloying elements contained in aluminum alloys significantly change the deformation process. Nanoparticles can lead to atypical dependences of changes in mechanical properties alloys but not pure metals. In the future, it will be necessary to consider the contribution of alloying elements and nanoparticles to the formation of the mechanical properties of the alloy.

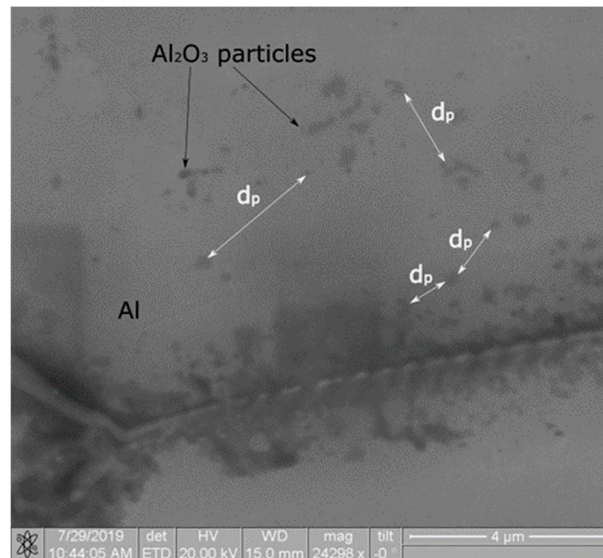


Figure 6. SEM image of the alloy sample with 1 wt.% Al_2O_3 .

6. Conclusions

This work has clearly shown that the addition of Al_2O_3 nanoparticles to commercial-purity aluminum promoted its structural refinement and reduced the average grain size from 200 to 69 μm .

This grain refinement and the addition of Al_2O_3 nanoparticles allowed us to increase the alloy hardness from 19.36 to 21.73 HBW, the yield stress from 12.08 to 27.4 MPa, and the ultimate tensile strength from 48.75 to 79.1 MPa. It was shown that the mechanical properties of pure aluminum depend mostly on two hardening mechanisms: The Orowan strengthening and the difference in thermal-expansion coefficients of the matrix and the particles. The contribution of these two mechanisms to precipitation hardening of the alloy sample with 1 wt.% Al_2O_3 was 36 and 20 MPa, respectively.

Author Contributions: Data curation, I.A.Z.; formal analysis, A.A.K., A.P.K. and M.G.K.; funding acquisition, I.A.Z.; investigation, A.A.K.; methodology, A.P.K.; supervision, A.B.V.; visualization, N.I.K., E.N.M. and D.V.L.

Funding: This research was funded by Russian Foundation for Basic Research grant number 18-38-20081.

Acknowledgments: The reported study was funded by RFBR according to the research project No 18-38-20081.

Conflicts of Interest: The authors declare no conflict of interest.

References

1. Malaki, M.; Xu, W.; Kasar, A.K.; Menezes, P.L.; Dieringa, H.; Varma, R.S.; Gupta, M. Advanced Metal Matrix Nanocomposites. *Metals* **2019**, *9*, 330. [[CrossRef](#)]
2. Promakhov, V.V.; Khmeleva, M.G.; Zhukov, I.A.; Platov, V.V.; Khrustalyov, A.P.; Vorozhtsov, A.B. Influence of Vibration Treatment and Modification of A356 Aluminum Alloy on Its Structure and Mechanical Properties. *Metals* **2019**, *9*, 87. [[CrossRef](#)]
3. De Luca, A.; Dunand, D.C.; Seidman, D.N. Mechanical properties and optimization of the aging of a dilute Al-Sc-Er-Zr-Si alloy with a high Zr/Sc ratio. *Acta Mater.* **2016**, *119*, 35–42. [[CrossRef](#)]

4. Spierings, A.B.; Dawson, K.; Heeling, T.; Uggowitz, P.J.; Schäublin, R.; Palm, F.; Wegener, K. Microstructural features of Sc- and Zr-modified Al-Mg alloys processed by selective laser melting. *Mater. Des.* **2017**, *115*, 52–63. [[CrossRef](#)]
5. Gao, T.; Ceguerra, A.; Breen, A.; Liu, X.; Wu, Y.; Ringer, S. Precipitation behaviors of cubic and tetragonal Zr-rich phase in Al-(Si-) Zr alloys. *J. Alloys Compd.* **2016**, *674*, 125–130. [[CrossRef](#)]
6. Shirvanimoghaddam, K.; Hamim, S.U.; Akbari, M.K.; Fakhrhoseini, S.M.; Khayyam, H.; Pakseresht, A.H.; Ghasali, E.; Zabet, M.; Munir, K.S.; Jia, S.; et al. Carbon fiber reinforced metal matrix composites: Fabrication processes and properties. *Compos. Part A Appl. Sci. Manuf.* **2017**, *92*, 70–96. [[CrossRef](#)]
7. Chen, B.; Shen, J.; Ye, X.; Jia, L.; Li, S.; Umeda, J.; Takahashi, M.; Kondoh, K. Length effect of carbon nanotubes on the strengthening mechanisms in metal matrix composites. *Acta Mater.* **2017**, *140*, 317–325. [[CrossRef](#)]
8. Maruyama, B.; Hunt, W.P. Discontinuously reinforced aluminum: Current status and future direction. *JOM* **1999**, *11*, 59–61. [[CrossRef](#)]
9. Umasankar, V.; Xavior, M.A.; Karthikeyan, S. Experimental evaluation of the influence of processing parameters on the mechanical properties of SiC particle reinforced AA6061 aluminium alloy matrix composite by powder processing. *J. Alloys Compd.* **2014**, *582*, 380–386. [[CrossRef](#)]
10. Khrustalyov, A.P.; Garkushin, G.V.; Zhukov, I.A.; Razorenov, S.V.; Vorozhtsov, A.B. Quasi-Static and Plate Impact Loading of Cast Magnesium Alloy ML5 Reinforced with Aluminum Nitride Nanoparticles. *Metals* **2019**, *9*, 715. [[CrossRef](#)]
11. Mirza, F.A.; Chen, D.L. A Unified Model for the Prediction of Yield Strength in Particulate-Reinforced Metal Matrix Nanocomposites. *Materials* **2015**, *8*, 5138–5153. [[CrossRef](#)] [[PubMed](#)]
12. Dieringa, H.; Katsarou, L.; Buzolin, R.; Szakács, G.; Horstmann, M.; Wolff, M.; Mendis, C.; Vorozhtsov, S.; StJohn, D. Ultrasound Assisted Casting of an AM60 Based Metal Matrix Nanocomposite, Its Properties, and Recyclability. *Metals* **2017**, *7*, 388. [[CrossRef](#)]
13. Casati, R.; Vedani, M. Metal Matrix Composites Reinforced by Nano-Particles—A Review. *Metals* **2014**, *4*, 65–83. [[CrossRef](#)]
14. Akbari, M.K.; Baharvandi, H.R.; Shirvanimoghaddam, K. Tensile and fracture behavior of nano/micro TiB₂ particle reinforced casting A356 aluminum alloy composites. *Mater. Des.* **2015**, *66*, 150–161. [[CrossRef](#)]
15. Katsarou, L.; Mounib, M.; Lefebvre, W.; Vorozhtsov, S.; Pavese, M.; Badini, C.; Molina-Aldareguia, J.M.; Jimenez, C.C.; Pérez Prado, M.T.; Dieringa, H. Microstructure, mechanical properties and creep of magnesium alloy Elektron21 reinforced with AlN nanoparticles by ultrasound-assisted stirring. *Mater. Sci. Eng. A* **2016**, *659*, 84–92. [[CrossRef](#)]
16. Sreekumar, V.M.; Babu, N.H.; Eskin, D.G. Prospects of In-Situ α -Al₂O₃ as an Inoculant in Aluminum: A Feasibility Study. *J. Mater. Eng. Perform.* **2017**, *26*, 4166–4176. [[CrossRef](#)]
17. Dieringa, H. Properties of magnesium alloys reinforced with nanoparticles and carbon nanotubes: A review. *J. Mater. Sci.* **2011**, *46*, 289–306. [[CrossRef](#)]
18. Puga, H.; Costa, S.; Barbosa, J.; Ribeiro, S.; Prokic, M. Influence of ultrasonic melt treatment on microstructure and mechanical properties of AlSi9Cu3 alloy. *J. Mater. Process. Technol.* **2011**, *211*, 1729–1735. [[CrossRef](#)]
19. Kudryashova, O.B.; Eskin, D.G.; Khrustalev, A.P.; Vorozhtsov, S.A. Ultrasonic effect on the penetration of the metallic melt into submicron particles and their agglomerates. *Russ. J. Non-Ferr. Met.* **2017**, *58*, 427–433. [[CrossRef](#)]
20. Zhang, F.; Jacobi, A.M. Aluminum surface wettability changes by pool boiling of nanofluids. *Colloids Surf. A Physicochem. Eng. Asp.* **2016**, *506*, 438–444. [[CrossRef](#)]
21. Vorozhtsov, S.; Zhukov, I.; Promakhov, V.; Naydenkin, E.; Khrustalyov, A.; Vorozhtsov, A. The Influence of ScF₃ Nanoparticles on the Physical and Mechanical Properties of New Metal Matrix Composites Based on A356 Aluminum Alloy. *JOM* **2016**, *68*, 3101–3106. [[CrossRef](#)]
22. Zhukov, I.A.; Kozulin, A.A.; Khrustalyov, A.P.; Matveev, A.E.; Platov, V.V.; Vorozhtsov, A.B.; Zhukova, T.V.; Promakhov, V.V. The Impact of Particle Reinforcement with Al₂O₃, TiB₂, and TiC and Severe Plastic Deformation Treatment on the Combination of Strength and Electrical Conductivity of Pure Aluminum. *Metals* **2019**, *9*, 65. [[CrossRef](#)]
23. Ramakrishnan, N. An analytical study on strengthening of particulate reinforced metal matrix composites. *Acta Mater.* **1996**, *44*, 69–77. [[CrossRef](#)]
24. Zhang, Z.; Chen, D.L. Consideration of Orowan strengthening effect in particulate-reinforced metal matrix nanocomposites: A model for predicting their yield strength. *Scr. Mater.* **2006**, *54*, 1321–1326. [[CrossRef](#)]

25. Zhang, Z.; Chen, D.L. Contribution of Orowan strengthening effect in particulate-reinforced metal matrix nanocomposites. *Mat. Sci. Eng. A* **2008**, *483–484*, 148–152. [[CrossRef](#)]
26. Shin, S.; Lee, D.; Lee, Y.-H.; Ko, S.; Park, H.; Lee, S.-B.; Cho, S.; Kim, Y.; Lee, S.-K.; Jo, I. High Temperature Mechanical Properties and Wear Performance of B4C/Al7075 Metal Matrix Composites. *Metals* **2019**, *9*, 1108. [[CrossRef](#)]
27. Khrustalyov, A.P.; Kozulin, A.A.; Zhukov, I.A.; Khmeleva, M.G.; Vorozhtsov, A.B.; Eskin, D.; Chankitmongkorn, S.; Platov, V.V.; Vasilyev, S.V. Influence of Titanium Diboride Particle Size on Structure and Mechanical Properties of an Al-Mg Alloy. *Metals* **2019**, *9*, 1030. [[CrossRef](#)]
28. Belov, N.A. Effect of eutectic phases on the fracture behavior of high-strength castable aluminum alloys. *Met. Sci. Heat Treat.* **1995**, *37*, 237–242. [[CrossRef](#)]
29. Chen, Z.; Wang, T.; Zheng, Y.; Zhao, Y.; Kang, H.; Gao, L. Development of TiB₂ reinforced aluminum foundry alloy based in situ composites—Part I: An improved halide salt route to fabricate Al–5 wt%TiB₂ master composite. *Mat. Sci. Eng. A* **2014**, *605*, 301–309. [[CrossRef](#)]
30. Vorozhtsov, S.A.; Eskin, D.G.; Tamayo, J.; Vorozhtsov, A.B.; Promakhov, V.V.; Averin, A.A.; Khrustalyov, A.P. The application of external fields to the manufacturing of novel dense composite master alloys and aluminum-based nanocomposites. *Metal. Mater. Trans. A* **2015**, *46*, 2870–2875. [[CrossRef](#)]



© 2019 by the authors. Licensee MDPI, Basel, Switzerland. This article is an open access article distributed under the terms and conditions of the Creative Commons Attribution (CC BY) license (<http://creativecommons.org/licenses/by/4.0/>).